High resolution absorption spectroscopy of the $\nu_1=2-6$ acetylenic overtone bands of propyne: Spectroscopy and dynamics

A. Campargue,[a] L. Biennier, A. Garnache, A. Kachanov, and D. Romanini
Laboratoire de Spectrométrie Physique (CNRS, UMR 5588), Université Joseph Fourier de Grenoble, B.P. 87, 38402 Saint Martin d'Hères Cedex, France

M. Herman
Laboratoire de Chimie Physique Moléculaire, CP 160/09, Université Libre de Bruxelles, Roosevelt Ave., 50, B-1050, Brussels, Belgium

(Received 5 April 1999; accepted 15 June 1999)

The rotationally resolved $n\nu_1$ ($n=2-6$) overtone transitions of the CH acetylenic stretching of propyne (CH_3–C≡C–H) have been recorded by using Fourier transform spectroscopy ($n=2$), various intracavity laser absorption spectrometers ($n=3$, 4, and 6) and cavity ring down spectroscopy (CRDS) ($n=5$). The $2\nu_1$, $3\nu_1$, and $6\nu_1$ bands exhibit a well-resolved and mostly unperturbed *J*-rotational structure, whose analysis is reported. The $5\nu_1$ band recorded by pulsed CRDS shows an unresolved rotational envelope. In the region of 12 700 cm^{-1}, an anharmonic interaction is confirmed between $4\nu_1$ and $3\nu_1+\nu_3+\nu_5$. The band at a higher wave number in this dyad exhibits a partly resolved *K*-structure, whose analysis is reported. The mixing coefficient of the two interacting states is determined consistently using different procedures. The 1/35 anharmonic resonance evidenced in the $4\nu_1$ manifold induces weaker intensity borrowing from the $2\nu_1$ and $3\nu_1$ levels to the $\nu_1+\nu_3+\nu_5$ and $2\nu_1+\nu_3+\nu_5$ level, respectively, which have been predicted and identified. Several hot bands around the $2\nu_1$, $3\nu_1$, and $3\nu_1+\nu_3+\nu_5$ bands arising from the $\nu_9=1$ and $\nu_{10}=1$ and 2 bending levels are identified and rotationally analyzed, also leading to determine $x_{1,9}$ [−20.3(3) cm^{-1}], $x_{1,10}$ [−1.7975(75) cm^{-1}], and $x_{3,10}$ [−6.56 cm^{-1}]. The *J*-clumps of the *P* and *R* branches in the $6\nu_1$ band at 18 499 cm^{-1} show a Lorentzian homogeneous profile mostly *J*-independent with an average full width at half maximum (FWHM) of 0.17 cm^{-1}, attributed to arising from the intramolecular vibrational energy redistribution towards the bath of vibrational states. A detailed comparative examination of the fine structure in all investigated $n\nu_1$ ($n=2$ to 7) overtone bands and the similar behavior of the cold and hot bands arising from $\nu_{10}=1$ definitively suggests that a highly specific low-order anharmonic coupling, still unidentified, dominates the hierarchy of interaction mechanisms connecting the $n\nu_1$ levels to the background states. © *1999 American Institute of Physics.* [S0021-9606(99)01334-3]

I. INTRODUCTION

The study of the mechanism of the vibrational energy flow is of fundamental interest to understand and model the pathways of redistribution of the vibrational excitation within an isolated molecule, named intramolecular vibrational redistribution (IVR) (see, for instance, Refs. 1–7). Ideally, it requires both time and state-resolved experiments, neither of which is easy to handle. Most of the investigations dealing with IVR in small and medium size molecules (see, for instance, Refs. 8–10) are, in fact, studies transposing in the time domain the experimental results obtained in the energy domain. Because of the size of the species investigated, such studies usually only provide information on the onset of IVR.

On the short time scale (typically less than 1 ps), IVR is ruled by strong anharmonic couplings connecting a state with strong zeroth-order bright character with a limited number of other states. For a number of small and medium size molecules, including acetylene[8] and CHX_3 species (X=D, F, Cl, CF_3, etc.),[9,10] a large set of highly selective anharmonic resonances could be identified. The C–H stretching vibrations have been extensively studied in this context because the corresponding overtone transitions dominate the absorption spectrum in the near infrared and visible ranges. In a direct absorption experiment, these particular transitions provide the ''key holes'' allowing the phase space to be explored. One should stress that only the phase space in the vicinity of the stretching bright state can be characterized from such studies and the resulting ''point of view'' may therefore be biased.

Weaker couplings, connecting the zeroth-order bright states to the so-called ''bath'' of vibrational dark states, govern the dynamics on a longer time scale. These couplings result in fine splitting or fractioning of the absorption lines. The intimate connection between the extent of IVR and the vibrational level density, previously assumed to be straightforward for larger species, is still to be better characterized using, in particular, the concept of a doorway state. Such states, introduced in particular in the tier model proposed by Stuchebrukhov, Mehta, and Marcus[11] provide a pathway for the energy to flow from the bright state to the bath of background states. These authors[11] have theoretically established

[a]Electronic mail: alain.campargue@ujf-grenoble.fr

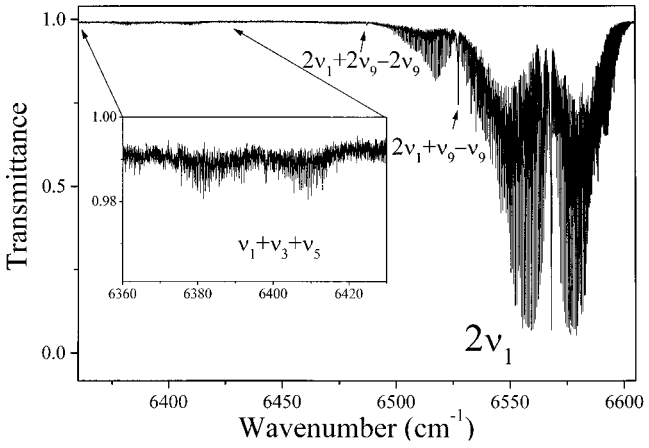

FIG. 1. Fourier transform spectrum of propyne in the region of the $2\nu_1$ overtone band recorded at a pressure of 43 hPa with an absorption pathlength of 240 cm.

that the relaxation of the acetylenic CH stretch excitation in $(CX_3)_3YCCH$ compounds is ruled by a sequence of off-resonance vibrational transitions between tiers coupled by low-order vibrational couplings.

Experimentally, state-selective spectroscopy at sub-Doppler resolution is ideally suited for IVR studies. A number of instrumental methods have been developed to probe the vibrational excited states labeled by a first laser: direct absorption from the excited level,[12,13] decrease of a resonant two-photon ionization signal,[14] microwave detected microwave-optical double resonance,[15] fluorescence signal from an electronic excited state, photofragment spectroscopies[16] including overtone spectroscopy by vibrationally assisted and photofragment ionization[17,18] and infrared laser assisted photofragment spectroscopy.[19–21] These techniques are generally less versatile than direct absorption methods, but they provide extremely detailed information which is highly valuable to indirectly probe the long time dynamics associated to the molecular overtone excitation. However, absorption spectroscopy carried at Doppler resolution and with a high sensitivity is a preliminary step suitable to have a global description of the couplings of the CH stretching modes.

Propyne (methyl acetylene) was chosen because previous investigations, in particular Ref. 22, have reported the observation of resolved and mostly unperturbed rotational structure at a very high excitation energy of the acetylenic CH-stretch, in energy regions where the vibrational density is as high as 10^7 states/cm^{-1}. This is probably unique case among the molecules of this size (7 atoms), which gives the opportunity to study how far this particular vibration is isolated from the rest of the molecule. The rovibrational absorption spectrum of propyne has been extensively investigated in the near infrared and visible ranges using the optoacoustic technique, by Hall,[22] Baylor *et al.*,[23] and Crofton *et al.*[24] Also, some of the $n\nu_1$ overtone transitions ($n=1-3$) presenting a fine structure were investigated in the literature using sub-Doppler resolution, in particular by Lehmann *et al.*[12,14,25,26] and by Perry *et al.*[27]

We recorded the overtone spectrum of propyne with highly sensitive experimental techniques, allowing the use of low-pressure samples and providing better resolved absorption spectra than previously. We focused on the $n\nu_1$ ($n=3-6$) overtone transitions using intracavity absorption spectroscopy (ICLAS) and cavity ring down spectroscopy (CRDS), under various instrumental configurations. The first overtone band ($n=2$) was also recorded, using Fourier transform spectroscopy (FTS). The experimental details are given in Sec. II. The quality of the data allowed us to investigate the fine structure of various bands *and* the vibrational energy pattern, in a much more detailed way than previously, leading to a significantly improved understanding of the spectroscopy. As a result, original information was obtained on the long- *and* short-time dynamics associated to the acetylenic CH stretching excitation, detailed in Secs. III and IV. In addition, we have attempted to interpret the observations related to cold and hot bands as revealing the role of doorway states. Indeed, we will show in Sec. III that important information is provided by the observed hot bands as the upper level of the cold band and the hot bands probe different energy regions of the vibrational background. In addition, it appears[22,28] that some of the $n\nu_1$ overtone transitions of the acetylenic CH stretching ($n=1-3$, 6, and 7) exhibit resolved rotational structure, while the $n=4$ and 5 levels in the intermediate range do not present any fine structure. The discussion of these striking observations, presented in Sec. IV, leads to relevant information on the relationship between the extent of IVR and the vibrational state density.

II. EXPERIMENTS

Different experimental setups were used in this study, which are detailed hereafter. A variety of laser systems, in particular, was employed at Grenoble University and generated most of the data of interest to the present investigation. FTS was used at Brussels University to record the near infrared spectrum over a broad spectral range. The latter information is, however, used here only in a limited number of case studies.

A. FTS

The FT spectrum was recorded from 4000 up to 8000 cm^{-1} using a Bruker IFS120HR interferometer equipped with a multipass cell set to 240 cm total absorption pathlength, and using an InSb detector and a CaF_2 beamsplitter. The resolution (defined as 0.9/total optical path difference) was 0.029 cm^{-1}, with Norton–Beer–Weak apodization. The pressure in the cell was 43 hPa and 256 scans were coadded. The transmittance spectrum was obtained by dividing the spectrum by one recorded under similar conditions, using an empty cell. Figure 1 presents the range of the $2\nu_1$ band, which is the only one from the FT data considered in the present study.

B. ICLAS

ICLAS is particularly well suited to explore large spectral regions with a routine sensitivity better than 10^{-8} cm^{-1}. The method is described in Ref. 29 and its applications reviewed and compared to the performance of other highly

TABLE I. Experimental conditions adopted for the recordings of the overtone transitions of propyne.

ν_1	Energy range (cm^{-1})			Pressure (hPa)			
2	4000–8000	FTS		43			
5	15 600–15 700	CRDS	Pulsed dye laser (DCM)	13.1			
					Generation time (μs)	l_{eq} (km)[a]	Reference lines
3	9600–9750	ICLAS	Multiple quantum wells VECSEL	less than 1	up to 200	up to 29.4	H_2O[b]
4	12 660–12 790		Dye laser (Styryl 8) and Ti:Sapphire	1–131	up to 400	up to 60	H_2O[b]
6	18 400–18 520		Dye laser (Rhodamine 110)	39–118	up to 350	up to 50.2	I_2[c]

[a]Obtained from $l_{eq}=(l/L)ct_g$ where l/L is the ratio of the length of the absorption cell to the optical length of the laser cavity.
[b]Reference 33.
[c]Reference 34.

sensitive laser techniques in Ref. 30. The intracavity cell filled with propyne (Lancaster, 98% stated purity) was inserted in the laser cavity. In the present experiments, we used three ICLAS systems to access the spectral regions of the $\nu_1=3-6$ overtone transitions. The first system uses our standard standing wave dye laser. The second system is a recently developed Ti:Sapphire ring cavity in a traveling wave configuration.[31] The third is a very promising development of ICLAS in the near- and mid-infrared regions based on the use of multiple quantum wells as vertical external cavity surface emitting semiconductor lasers (VECSELs).[32] Compared to previous investigations in our group, the data acquisition system has been upgraded using a 3724-pixels charge coupled device (CCD) to record the laser spectrum dispersed by the grating spectrograph. This setup allows 15 cm^{-1} broad sections of the laser spectrum to be recorded with higher spectral resolution (resolving power 8×10^5). Table I summarizes the experimental conditions adopted for the recording of each band. The wave number calibration procedure consists, first, of correcting the nonlinear dispersion of the spectrograph by using a BK7 etalon inserted into the ICLAS laser and giving sharp fringes equidistant in frequency. Absolute calibration followed using the reference lines either from atmospheric water vapor ($\nu_1=3$, 4) or from iodine ($\nu_1=6$) as indicated in Table I. We estimate our wave number calibration to be precise to within 0.01 cm^{-1} as confirmed by the ground-state combination differences provided by the following rotational analysis.

C. CRDS

The $5\nu_1$ band shows unresolved structure, as already reported by Hall.[22] It could not, therefore, be recorded using the ICLAS technique, which is unable to reproduce broad features. Indeed, with ICLAS, absorption continua are simply added to broadband losses, such as those arising from the output coupler transmission and from losses on mirrors and intracavity elements. They are compensated by laser gain and result only in a higher threshold which cannot be measured.

We therefore used CRDS. The technique is introduced in the earlier work of O'Keefe and Deacon[35] and reviewed in Refs. 30 and 36, for instance. CRDS is highly versatile. It can achieve sub-Doppler recording[37] as well as measure broadband absorption. For instance, a 40 cm^{-1} wide unresolved broad overtone transition could be recorded in CHF_3, using CRDS with a diode laser.[38] In addition, CRDS is ultrasensitive, even for the recording of broadband spectra. For instance, it allowed some of us to detect the broad absorption spectrum of an electronic transition in an ionized polycyclic aromatic hydrocarbon ($C_8H_{10}^+$) in the gas phase, using a slit jet setup combined with an electronic discharge.[39]

The CRDS spectrum of the $5\nu_1$ band of propyne recorded at a pressure of 10 Torr is displayed in Fig. 2. It was obtained from the difference in decay rate measured with and without the absorber in the cavity. The time interval between these successive scans was minimized in order to avoid baseline bias resulting from drift of the pulsed laser beam. The pulsed dye laser was partially mode-matched to the cavity, and a detection limit of better than 10^{-7} per pass was achieved averaging the ring down rate over 10 to 20 laser shots. The instrumental resolution was better than 0.2 cm^{-1}. The value of the wavelength was given by the sine-drive mechanism of our dye laser (Lambda Physik), after recali-

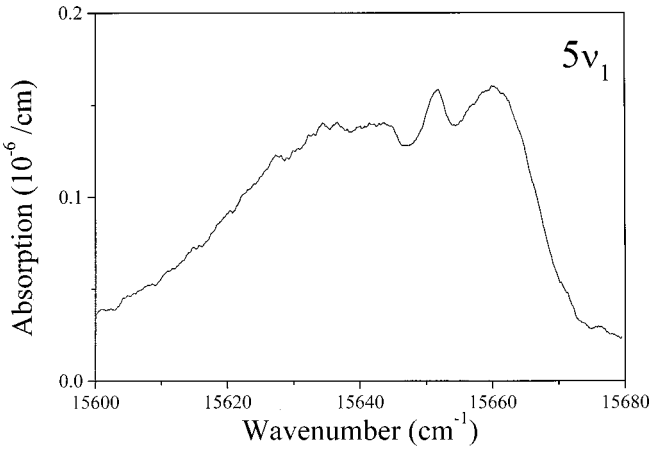

FIG. 2. Pulsed CRDS spectrum of the $5\nu_1$ overtone band of propyne recorded at a pressure of 10 Torr (13.1 hPa). The effective resolution was about 0.2 cm^{-1}.

bration using a hollow cathode spectral lamp. This method is accurate enough in the present case, given the structureless character of the $5\nu_1$ band.

III. SPECTROSCOPY

A. General features

All overtone transitions we consider in this work correspond to the excitation of an upper state of A_1 symmetry, from the ground state. Only hot bands, which we also consider, involve states with E symmetry. The rotational energy in A_1 states is given by the standard relation

$$F(J,K)=\nu_0+BJ(J+1)+(A-B)K^2-D_JJ^2(J+1)^2 - D_{JK}J(J+1)K^2-D_KK^4. \quad (1)$$

We are thus dealing with A_1-A_1 parallel transitions in the C_{3v} symmetry group which follow the selection rules $\Delta J=0,\pm1$ and $\Delta K=0$. Each of the $P(J)$ and $R(J)$ lines is actually a clump of lines composed by a fine K-structure governed by the term $(\Delta A-\Delta B)K^2$.

Two remarks will help in the following rotational analysis. In the first place, the A principal rotational constant is the one related to the acetylenic molecular axis, i.e., the same axis as the one on which the acetylenic CH vibration, ν_1, occurs. The value of α_1^A describing the linear dependence of A with the ν_1 quantum number is therefore expected to be extremely weak. This intuitive prediction is confirmed by force field calculations[25] which obtained $\alpha_1^A=2\times10^{-6}$ cm^{-1}. The K-structure in the $n\nu_1$ bands is then governed by $(-\Delta BK^2)$ and blue-degraded as $\Delta B<0$.

Second, the relative intensity of the K lines within a $P(J)$ and a $R(J)$ clump can be calculated from the product of the Hönl–London factor, the nuclear spin weights (which is 2 when K is a multiple of 3, and 1 otherwise), and the Boltzmann factor. It is such that, at room temperature, in a J-clump with $J>10$, more than 85% of the intensity is carried by the transitions with $K\leqslant6$. This is mainly due to the large value of A in the ground state (5.3 cm^{-1}), which makes the population factor decrease very quickly with K. As a consequence, the additional K-lines appearing for higher J values do not bring significant extra intensity and one can thus expect the $P(J)$ and $R(J)$ clumps to exhibit an almost unchanged profile for $J>7$. Only the transition wave numbers of the $3\nu_1+\nu_3+\nu_5$ band are listed in this paper, as this band is very peculiar and exhibits a partly resolved K-structure. The wave numbers of the lines in the other bands which have been rotationally analyzed ($3\nu_1$, $6\nu_1$, $3\nu_1+\nu_9-\nu_9$, $3\nu_1+\nu_{10}-\nu_{10}$, and $3\nu_1+\nu_3+\nu_5+\nu_{10}-\nu_{10}$) are available on request from the first author.

B. The $3\nu_1$ band

An overview of the ICLAS spectrum in the range of the $3\nu_1$ band centered at 9702.43 cm^{-1} is displayed in Fig. 3. The $3\nu_1$ band is accompanied by the $3\nu_1+\nu_{10}-\nu_{10}$ and $3\nu_1+2\nu_{10}-2\nu_{10}$ hot bands at 9696.94 and 9691.38 cm^{-1}, respectively, and by two weaker bands lying at 9642.1 and 9614.9 cm^{-1} which will be discussed later in this paper. The main band was previously reported by Herzberg *et al.*[40] and

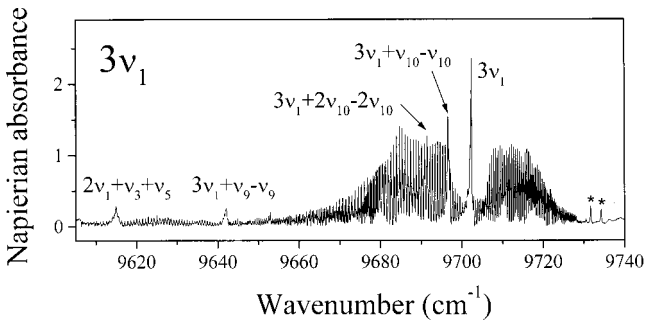

FIG. 3. Overview of the ICLAS spectrum of propyne in the range of the $3\nu_1$ overtone band. The spectrum was recorded with a new type of ICLAS spectrometer using VECSEL as the amplification medium. The two lines marked with a sign * on the higher-energy part of the spectrum are due to atmospheric water absorption. The pressure of propyne in the intracavity cell was about 1.3 hPa and the equivalent absorption pathlength 14.7 km.

by Badger and Bauer,[41] who obtained photographic infrared plates exhibiting well-resolved J-rotational structure. Later, Hall[22] recorded the Fourier transform spectrum of the $3\nu_1$ band at a pressure of 300 Torr and reported the rotational analysis of the J-structure. The relatively high pressure and the limited resolution (0.07 cm^{-1}) used in all these previous recordings prevented the observation of the K-structure. As mentioned in the experimental section, the ICLAS spectrum was obtained with a newly built spectrometer using multiple quantum wells as an amplification medium. In the present experiment, we unfortunately could not use our higher resolution grating spectrograph, and therefore the experimental resolution was limited to 0.1 cm^{-1} (FWHM). Nevertheless, as illustrated in Fig. 4, the $P(J)$ lines with J-values larger than 17 appear to be divided into two or three components with energy spacing changing slowly with J. We repeated Hall's analysis,[22] again only considering the J-rotational structure and using the expression for a linear molecule, thus neglecting the K-structure

$$F(J,K)=\nu_0+BJ(J+1)-D_JJ^2(J+1)^2. \quad (2)$$

The ground-state values of B and D_J were held to their literature values.[42] We performed two separate fits, whose results are given in Table II. The first set of constants in Table II (fit 1) corresponds to the results obtained by fitting the lines with low J-values ($J<17$), which appear as structure-

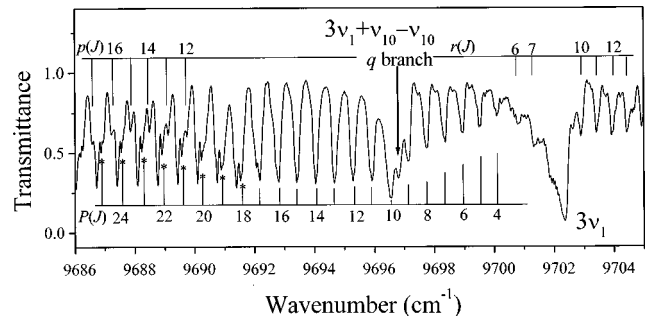

FIG. 4. Portion of the ICLAS spectrum of propyne showing the $3\nu_1$ cold band and the $3\nu_1+\nu_{10}-\nu_{10}$ hot band with their respective rotational assignment. The $p(J)$ and $r(J)$ rotational assignments of the hot band are given in the upper part. The $P(J)$ lines of $3\nu_1$ marked with a star were included in fit 2 (see the text and Table II).

TABLE II. Rovibrational parameters of some overtone bands of propyne. All values are given in cm^{-1}.

	G_v	B	$D_J\times10^{-8}$		Ref.
Ground state	0	0.285 059 767	9.803 545 8		42
ν_9	638.569 14	0.285 232 59	9.845 22		47
ν_{10}	330.938 55	0.285 858 422	10.052 4		48
	ν_0	$\Delta B\times10^{-3}$	$\Delta D_J\times10^{-8}$	Lines[a]	σ[b]$\times10^{-3}$
$3\nu_1$ (fit 1)[c]	9702.420(4)	−2.17(2)	0[e]	23(75)	18.8
$3\nu_1$ (fit 2)[d]	9702.428(4)	−2.19(1)	2.2(5)	69(75)	17.6
$3\nu_1$ (Ref. 22)	9702.401(22)	−2.15(13)	51(17)	47(70)	
$3\nu_1$ (Ref. 40)	9702.30	−2.41(10)			
$3\nu_1+\nu_9-\nu_9$	9642.065(4)	−2.04(3)	77(4)	36(39)	16.4
$3\nu_1+\nu_{10}-\nu_{10}$	9696.916(2)	−2.342(9)	0[e]	16(16)	7.2
$3\nu_1+\nu_3+\nu_5$[f]	12 764.238(1)	−4.454(3)	−2.48(8)	190(201)	9.0
$3\nu_1+\nu_3+\nu_5+\nu_{10}-\nu_{10}$[g]	12 755.115(3)	−4.375(9)	−3.4(5)	58(63)	12.8
$3\nu_1+\nu_3+\nu_5+\nu_{10}-\nu_{10}$[g]	12 754.970(5)	−4.48(2)	−19(3)	28(30)	10.3
$3\nu_1+\nu_3+\nu_5+\nu_{10}-\nu_{10}$ (Ref. 28)	1 2755.13	−4.36			
$6\nu_1$	18 499.129(2)	−4.534(8)	14.9(6)	67(84)	7.8

[a]Number of lines included in the fitting procedure with, in parentheses, the total number of assigned lines.
[b]Root mean square deviation.
[c]Lines with $J''>17$ were excluded from the preceding fit 1. Higher J-values corresponding to the weak component of the doublets (see Fig. 2) were included in fit 2 (see the text).
[d]Lines with $J''>17$ were excluded from fit 1 and included in fit 2. The higher J-values included in fit 2 were those corresponding to the weak component of the doublets (see Fig. 4 and the text).
[e]Constrained to zero.
[f]See also Table V.
[g]The constants in the first line were obtained by fitting the line positions of the weak component of the observed doublet and those of the second line by fitting the line positions of the strongest component in the same doublets (see Fig. 9).

less clumps in our spectrum. The second set of parameters (fit 2) has been obtained by adding in the fit the components marked with the sign $*$ in Fig. 4. These peaks, although not the strongest within each clump and probably characterizing different K-values from one clump to another, correspond best to the line position extrapolated from the first set of parameters. In this way, we could include 69 line positions in fit 2 with a standard deviation of 0.018 cm^{-1}.

The resulting values of the rovibrational parameters confirm and refine those obtained by Hall[22] and by Herzberg *et al.*[37] However, as the K-structure is barely resolved and probably perturbed, the values of these parameters must be considered as effective. Indeed, the standard deviation of the rotational fit is 0.018 cm^{-1}. This is larger than the line positions uncertainty and reveals the presence of some perturbations. Gambogi *et al.*[13] have recorded, by eigenstate double-resonance spectroscopy, the spectrum corresponding to the $K=0$ and 1 subbands of the $J=0-4$ clumps with sub-Doppler resolution. Besides line fractioning that will be discussed later, they reported and discussed an extremely large splitting of about 0.1 cm^{-1} between the $K=0$ and $K=1$ levels in a direction opposite than expected.[13] This perturbation was assigned to z-axis Coriolis coupling of the $3\nu_1$ state with some background states, mediated by at least one nonresonant doorway state. Strong perturbations in the K-structure were also highlighted in the literature for the ν_1[25] and $2\nu_1$[12] bands.

C. The $6\nu_1$ band

An overview of the ICLAS spectrum of the $6\nu_1$ parallel band is given in Fig. 5. To our knowledge, the only previous study of this band was performed by Hall.[22] This author, however, only presented a plot of the band with a resolved J-rotational structure and did not provide rotational assignments and constants. As we shall discuss below, the width of the rotational lines of the $6\nu_1$ band is affected by a homogeneous broadening resulting from a strong line fractioning. This broadening is of about 0.2 cm^{-1} (FWHM) and prevents resolving the K-structure. As for the $3\nu_1$ band, we used Eq. (2) to determine the rovibrational parameters. They are also listed in Table II. Sixty-seven line positions could be reproduced with a rms deviation of 7.8×10^{-3} cm^{-1}, i.e., close to the experimental uncertainty. Only a limited number of lines

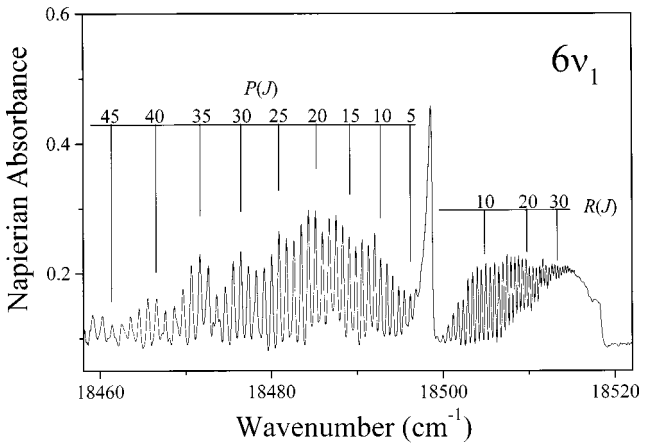

FIG. 5. Overview of the ICLAS spectrum of propyne in the range of the $6\nu_1$ overtone transition. The pressure in the intracavity cell was 60 Torr (78.6 hPa) and the equivalent absorption pathlength 23.5 km.

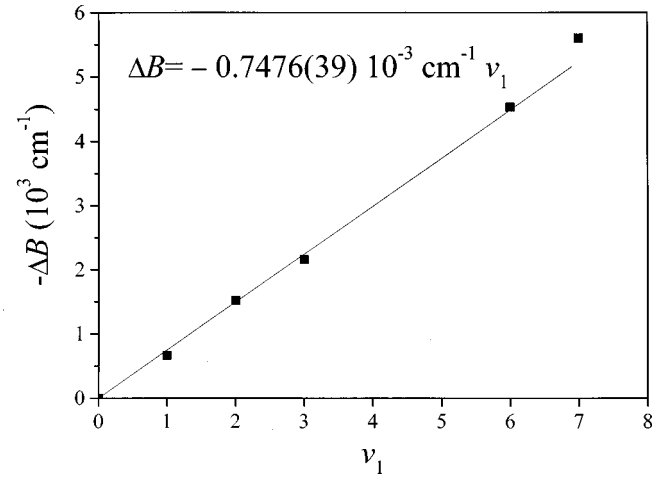

FIG. 6. Variation of the principal rotational constant ΔB (in cm^{-1}) versus the ν_1 stretching quantum number, in propyne. The values for $\nu_1=1$ (-6.65×10^{-4} cm^{-1}), $\nu_1=2$(-1.52×10^{-3} cm^{-1}), and $\nu_1=7$(-5.60×10^{-3} cm^{-1}) were taken from Refs. 25, 12 and 22, respectively. The latter value was not included in the fit discussed in the text.

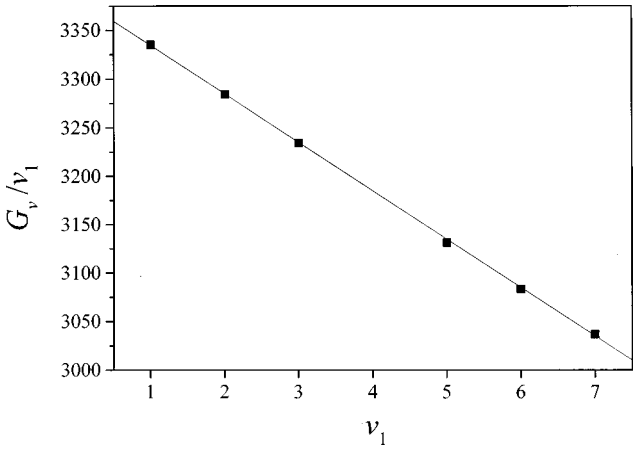

FIG. 7. Birge–Sponer plot for the CH acetylenic stretch levels of propyne. The vibrational term values for $\nu_1=1$ (3335.066 cm^{-1}), $\nu_1=2$ (6568.171 cm^{-1}), and $\nu_1=7$ (21 256.699 cm^{-1}) were taken from Refs. 25, 12, and 22, respectively. The energy of the $\nu_1=1$, 2, 3, and 6 levels is reproduced with a standard deviation of 0.36 cm^{-1} by an expression of the form $3384.924\nu_1-50.289\nu_1^2$.

corresponding to high J-values ($J>35$), which were not included in the fit, are not reproduced satisfactorily.

Figure 6 shows the linear dependence of the ΔB value versus the ν_1 quantum number. The fit including the $\nu_1=1$, 2, 3, and 6 data gives $\alpha_B^1=-0.7476(39)10^{-3}$ cm^{-1} in reasonable agreement with force-field predictions[25] ($\alpha_B^1=-0.623\times10^{-3}$ cm^{-1}). Figure 7 shows the corresponding Birge–Sponer plot. A closer look would show that, while the energy of the $\nu_1=6$ level coincides with the value extrapolated from those of the $\nu_1=1$ to 3 levels, deviations as large as -11 and 26.4 cm^{-1} are observed for the $\nu_1=5$ and $\nu_1=7$[22] levels, respectively. The expression $\tilde{\nu}_1\nu_1+x_{11}\nu_1^2$ for the vibrational term value allowed the effective vibrational wave number ($\tilde{\nu}_1$) and anharmonicity (x_{11}) of the acetylenic CH stretch to be determined as 3384.924(51) cm^{-1} and $-50.289(9)$ cm^{-1}, respectively. Using those constants, the energy of the $\nu_1=1$, 2, 3, and 6 levels is reproduced with a standard deviation of 0.36 cm^{-1} (see Table III).

The vibrational analysis of the $6\nu_1$ band therefore confirms the results of the rotational one, concerning the absence of strong perturbation. The $\nu_1=6$ level behaves, to a very large extent, as a pure acetylenic stretching state, largely decoupled from the other vibrational states. This situation is strikingly different from that of the $\nu_1=4$, 5, and, to a lesser

TABLE III. Calculated and observed vibrational term value (in cm^{-1}) for the $n\nu_1$ and $(n-1)\nu_1+\nu_3+\nu_5$ levels of propyne.

	$n\nu_1$			$(n-1)\nu_1+\nu_3+\nu_5$		Δ^h
n	Obs.	Obs.-Calc.		Obs.	Calc.	
		I[f]	II[i]		II[i]	
1	3335.066[a]	0.43	1.50	⋯	3067.72	265.0
2	6568.171[b]	−0.52	0.38	6398.05[g,c]	6393.53	171.6
3	9702.402[c]	0.23	−2.04	9614.9[c]	9617.32	67.8
4	12712[c,d]		−6.70	12764.24[c]	12763.87	−15.1
5	15 656.43[c]	−11.0	−6.2	⋯	15781.15	−108.5
6	18 499.129[c]	−0.01	0.61	⋯	18706.89	−201.9
7	21 256.699[e]	26.4	23.2	⋯	21533.93	−295.2

[a]Reference 25.
[b]Reference 12.
[c]This work.
[d]Value of the (mixed) $4\nu_1$ level strongly affected by the 1/35 anharmonic interaction with $3\nu_1+\nu_3+\nu_5$.
[e]Reference 22.
[f]The calculated values were determined from $G_\nu=3384.924\nu_1-50.289\nu_1^2$ obtained from the fit of the ν_1, $2\nu_1$, $3\nu_1$ and $6\nu_1$ energy levels.
[g]Q branch maximum absorption.
[h]Difference between the calculated energies of the $n\nu_1$ and $(n-1)\nu_1+\nu_3+\nu_5$ zeroth-order states.
[i]The calculated values were obtained taking into account the 1/35 anharmonic interaction for all pairs of levels. The value of $K_{1,35}$ (30.1 cm^{-1}) was constrained to the value determined for the $n=4$ pair (see the text) while $\tilde{\nu}_3+\tilde{\nu}_5=3068.15$ cm^{-1} was obtained from the literature (Refs. 45, 46). The three parameters (in cm^{-1}) $\tilde{\nu}_1$ (3383.04), x_{11} (-49.90), and $x_{13}+x_{15}$ (-6.43), were fitted in order to reproduce the six levels of the $n=1-3$ dyads and the $6\nu_1$ level.

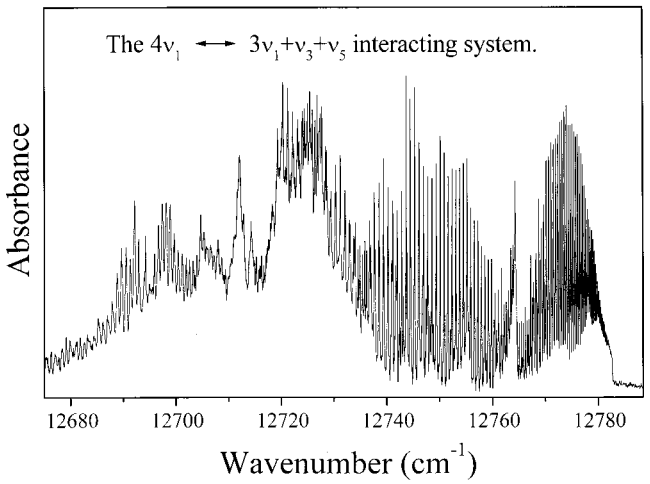

FIG. 8. Overview of the ICLAS spectrum of propyne in the region of the $4\nu_1$ transition. The spectrum was recorded at a pressure of 17 hPa with an equivalent absorption pathlength of 27 km. The observed spectrum results from an anharmonic interaction between the zeroth-order $4\nu_1$ bright level and the zeroth-order $3\nu_1+\nu_3+\nu_5$ combination level. The baseline in case of broad absorption features, such as encountered here for the $4\nu_1$ band, cannot be measured reliably by ICLAS. It was estimated using the spectrum published in Ref. 22.

extent, $\nu_1=7$ states, whose rotational and/or vibrational energies are strongly affected by a number of perturbations, as discussed hereafter.

D. The $4\nu_1 \leftrightarrow 3\nu_1+\nu_3+\nu_5$ interacting system

In the range where the $4\nu_1$ band is predicted to be observed, the absorption spectrum is dominated by two bands centered at 12 712 and 12 764 cm^{-1}. Figure 8 shows an overview of these two bands. Due to strong baseline uncertainties in an ICLAS experiment, the baseline of the unresolved part

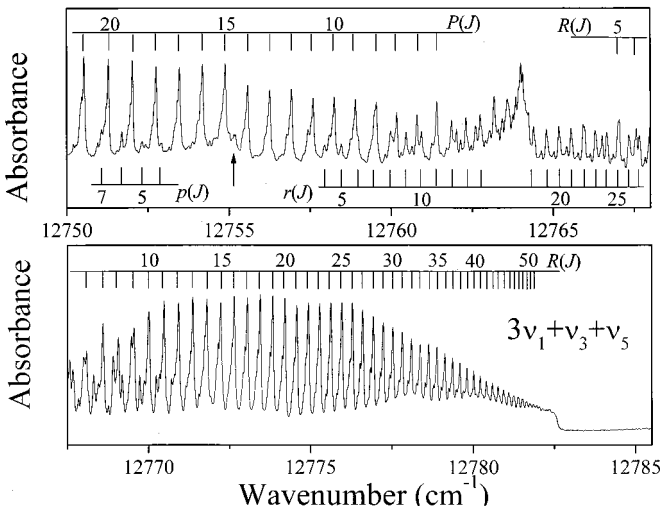

FIG. 9. Part of the $3\nu_1+\nu_3+\nu_5$ combination band of propyne recorded at a pressure of 17.3 hPa with an equivalent absorption pathlength of 18 km. The *J*-rotational assignment is given for the cold band $[P(J)$ and $R(J)]$ and for the $3\nu_1+\nu_3+\nu_5+\nu_{10}-\nu_{10}$ hot band $[p(J)$ and $r(J)]$. The arrow in the upper spectrum indicates the hot band center at 12755.11 cm^{-1}. The doublet fine structure of this hot band is clearly observed in the *R* branch just above the *Q* branch of the cold band.

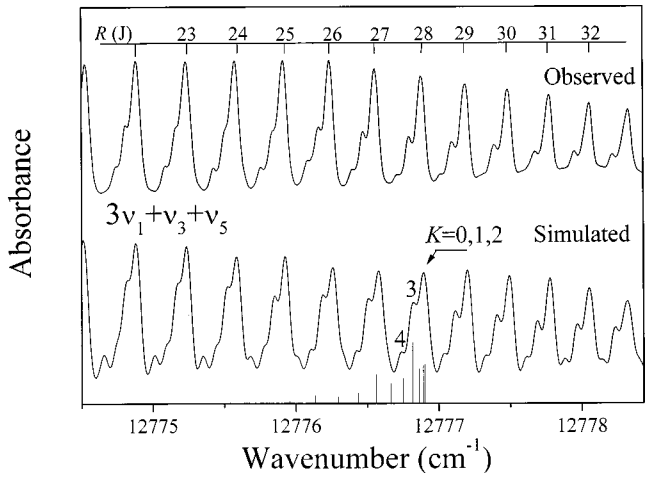

FIG. 10. Comparison of the observed (upper) and simulated (lower) spectrum of a section of the *R* branch of the $3\nu_1+\nu_3+\nu_5$ combination band in propyne. Note that the $K=5$ subband is perturbed and not observed in the ICLAS spectrum as a result of an energy perturbation of this subband. The stick spectrum corresponds to the simulated *K*-structure of the $R(28)$ transition.

of the spectrum was estimated with the help of the spectrum given in Ref. 22. The low-energy component is stronger and exhibits almost unresolved broadened lines appearing superimposed on a broad unresolved envelope. The second band shows a rotationally resolved spectrum at room temperature whose *J*-structure was partly analyzed by Hall[22] and later by Lin *et al.*[28] Figure 9 shows the high-energy part of the ICLAS spectrum of this band whose partly resolved *K*-structure will be analyzed below. The vibrational assignment of these two bands, $4\nu_1$ and $3\nu_1+\nu_3+\nu_5$, was established by Crofton *et al.*[24] on the basis of the relative intensity of these bands and of the comparison of their center with the predicted energy of the $4\nu_1$ band center. The modes ν_3 (2128 cm^{-1}, A_1) and ν_5 (930 cm^{-1}, A_1) are the C≡C and C–C stretching modes, respectively. These two anharmonically coupled bands form a dyad. The $4\nu_1$ character is dominant for the level participating in the strongest band, at 12 712 cm^{-1}. For simplicity, in the text we label the eigenstates using their dominant zeroth-order character.

1. Rotational analysis of the combination band at 12 764 cm^{-1}

As previously mentioned, in the *P* and *R* branches, a fine structure governed by the $(\Delta A-\Delta B)K^2$ term is expected for each *J*-value. As shown in Fig. 10, the *K*-structure is only partly resolved and the *K*-assignment is not straightforward. Indeed, if we consider the $P(J+1,K)$ and $R(J-1,K)$ transitions reaching the same upper (J,K) rotational level, ground-state combination differences of the type $R(J-1,K)-P(J+1,K)$ for the different *K*-values of the clump differ only by the term $D_{JK}K^2(J+1)^2$ [see Eq. (1)]. The contribution of this term is much too small compared to the precision of the wave number measurements to discriminate between different *K*-values. The *K*-assignment was deduced by assuming unperturbed relative intensity within a given clump. Using this procedure, we assigned the strongest absorption peak in each *J*-clump to $K=0$ and the line appear-

TABLE IV. Observed line positions of the $3\nu_1+\nu_3+\nu_5$ band of propyne (in cm^{-1}) and observed–calulated values.

J	K	$P(J)$	Obs–calc	J	K	$P(J)$	Obs–calc
1	0	12 763.672	0.004	38	0	12 736.385	0.003
2	0	12 763.082	−0.007	39	0	12 735.483	0.002
3	0	12 762.502	0.001	40	0	12 734.570	−0.001
4	0	12 761.907	0.003	41	0	12 733.654	0.002
5	0	12 761.296	−0.003	42	0	12 732.729	0.003
5	4	12 761.140*	−0.030	43	0	12 731.790	−0.001
5	6	12 760.969*	−0.040	44	0	12 730.838	−0.011
6	0	12 760.682	−0.002	45	0	12 729.905	0.008
7	0	12 760.060	0.000	46	0	12 728.961	0.024
8	0	12 759.426	−0.002	47	0	12 727.962	−0.008
8	3	12 759.380*	0.025	48	0	12 726.996	0.002
9	0	12 758.783	−0.004	49	0	12 726.018	0.008
10	0	12 758.137	0.000	50	0	12 725.018	0.000
10	4	12 757.995	−0.011	51	0	12 724.009	−0.009
11	0	12 757.476	−0.002	52	0	12 726.006	−0.004
11	4	12 757.330	−0.017	53	0	12 721.983	−0.011
11	6	12 757.179	−0.004	54	0	12 721.000	0.030
12	0	12 756.802	−0.008	57	0	12 711.851	0.001
12	4	12 756.672	−0.006	58	0	12 716.817	0.023
12	6	12 756.520	0.007	59	0	12 715.735	0.004
13	0	12 756.124	−0.009	60	0	12 714.662	0.002
13	3	12 756.057	−0.002				
14	0	12 755.442	−0.006	J	K	$R(J)$	Obs–calc
15	0	12 754.745	−0.008	1	0	12 765.339	−0.013
16	0	12 754.041	−0.009	2	0	12 765.890	−0.005
16	6	12 753.741	−0.004	3	0	12 766.432	0.003
17	0	12 753.328	−0.010	4	0	12 766.955	0.000
17	6	12 753.013	−0.018	5	0	12 767.483	0.012
18	0	12 752.604	−0.014	6	3	12 767.907*	0.002
18	6	12 752.284	−0.024	6	0	12 767.991	0.012
19	0	12 751.873	−0.015	7	6	12 768.210*	0.031
20	0	12 751.133	−0.017	7	4	12 768.363	0.018
20	3	12 751.079	0.008	7	0	12 768.496	0.018
21	0	12 750.386	−0.017	8	6	12 768.663	−0.004
21	3	12 750.320	−0.003	8	4	12 768.812*	−0.022
21	6	12 750.068	−0.016	8	0	12 768.971	0.003
22	0	12 749.632	−0.016	9	3	12 769.373	−0.001
22	4	12 749.503	−0.001	9	0	12 769.456	0.007
22	6	12 749.310	−0.015	10	4	12 769.771	−0.014
23	0	12 748.872	−0.011	10	0	12 769.919	−0.003
23	6	12 748.549	−0.008	11	6	12 770.147*	0.071
24	0	12 748.097	−0.013	11	4	12 770.257	0.009
24	6	12 747.767	−0.013	11	3	12 770.321	0.013
25	0	12 747.341	0.013	11	0	12 770.388	0.004
25	3	12 747.236	−0.008	12	6	12 770.626*	0.098
25	6	12 747.010	0.016	12	4	12 770.712	0.011
26	0	12 746.524	−0.013	12	3	12 770.775	0.014
26	4	12 746.388	0.001	12	0	12 770.841	0.002
27	0	12 745.744	0.005	13	6	12 771.073*	0.103
27	3	12 745.666	0.013	13	4	12 771.155	0.010
27	6	12 745.407	0.010	13	3	12 771.215	0.009
28	0	12 744.937	0.007	13	0	12 771.283	−0.001
28	4	12 744.796	0.020	14	6	12 771.478*	0.074
28	6	12 744.581	0.003	14	4	12 771.602	0.022
29	0	12 744.116	0.002	14	3	12 771.656	0.014
30	0	12 743.292	0.003	14	0	12 771.722	0.001
30	0	12 742.454	−0.002	15	4	12 772.026	0.019
32	0	12 741.610	−0.003	15	3	12 772.076	0.007
32	4	12 741.456	0.005	15	0	12 772.148	0.000
33	0	12 740.776	0.014	16	4	12 772.440	0.016
34	0	12 739.916	0.013	16	3	12 772.495	0.009
34	3	12 739.806	−0.003	16	0	12 772.567	0.000
35	0	12 739.037	0.001	17	6	12 772.700*	0.050
36	0	12 738.163	0.003	17	4	12 772.848	0.016
36	3	12 738.059	−0.003	17	3	12 722.905	0.009
37	0	12 737.279	0.004	17	0	12 772.978	0.001

TABLE IV. (*Continued.*)

J	*K*	*R*(*J*)	Obs−calc	*J*	*K*	*R*(*J*)	Obs−calc
18	4	12 773.254	0.023	32	0	12 778.072	0.000
18	3	12 773.302	0.006	33	4	12 778.155	−0.005
18	0	12 773.380	0.002	33	3	12 778.232	−0.007
19	3	12 773.692	0.004	33	0	12 778.342	0.001
19	0	12 773.774	0.003	34	3	12 778.494	−0.005
20	3	12 774.074	0.004	34	0	12 778.602	−0.001
20	0	12 774.156	0.002	35	3	12 778.746	−0.003
21	3	12 774.449	0.005	35	0	12 778.856	0.000
21	0	12 774.527	−0.002	36	3	12 778.986	−0.006
22	4	12 774.748	0.008	36	0	12 779.100	0.001
22	3	12 774.814	0.006	37	3	12 779.221	−0.004
22	0	12 774.889	−0.006	37	0	12 779.337	0.002
23	0	12 775.242	−0.010	38	3	12 779.450	−0.001
24	4	12 775.439	−0.002	38	0	12 779.563	0.001
24	0	12 775.589	−0.011	39	3	12 779.671	0.004
25	4	12 775.773	−0.006	39	0	12 779.781	0.001
25	0	12 775.930	−0.010	40	0	12 779.991	0.001
26	4	12 776.109	0.002	41	0	12 780.190	−0.001
26	3	12 776.187	0.008	42	0	12 780.382	−0.002
26	0	12 776.262	−0.009	43	0	12 780.567	−0.002
27	4	12 776.427	0.000	44	0	12 780.744	−0.001
27	3	12 776.502	−0.003	45	0	12 780.913	0.001
27	0	12 776.583	−0.009	46	0	12 781.075	0.004
28	4	12 776.736	−0.001	47	0	12 781.226	0.004
28	3	12 776.813	0.002	48	0	12 781.369	0.004
28	0	12 766.897	−0.009	49	0	12 781.505	0.006
29	4	12 777.036	−0.003	50	0	12 781.629	0.004
29	3	12 777.112	−0.002	51	0	12 781.738	−0.004
29	0	12 777.204	−0.007	52	0	12 781.847	−0.006
30	3	12 777.406	−0.002	53	0	12 781.945	−0.009
30	0	12 777.500	−0.006	54	0	12 782.032	−0.015
31	4	12 777.613	−0.004	55	0	12 782.126	−0.005
31	3	12 777.692	−0.002	56	0	12 782.192	−0.017
31	0	12 777.790	−0.004	57	0	12 782.264	−0.014
32	4	12 777.906	0.014	58	0	12 782.344	0.005
32	3	12 777.966	−0.005				

ing systematically just below in energy to $K=3$. A total of 201 lines (listed in Table IV) was assigned by this way to $K=0$, 3, and 4 for *J*-clumps with *J*-values up to 60. The corresponding wave numbers were included in a least-square fit and the rovibrational parameters determined using Eq. (1). They are listed and compared to previous literature results in Table V. The present parameters allow 190 line positions to be reproduced with a rms value of 7×10^{-3} cm^{-1}, i.e., close to experimental precision. A number of lines have been tentatively assigned to $K=6$ because of the good agreement of the observed and calculated wave number values. Indeed, the simulated spectrum, given in Fig. 10, agrees reasonably well with the observation except for the $K=5$ subband, which is not observed in the experimental spectrum. This type of perturbation affecting one *K*-subband is a common feature[25] in symmetric-top molecules with a large value of the *A* rotational constant such as propyne. The acetylenic stretching fundamental[25] and lower energy states in propyne itself[43–45] show beautiful examples of such perturbations. For instance, the different *K*-subbands of the ν_1 fundamental appear not to be perturbed but the ordering of the subband origins are perturbed through nonresonant interactions. The interaction responsible for the perturbations of these *K*-subbands has been identified[25] as resulting from the anharmonic coupling between the CH acetylenic level and a *z*-axis Coriolis mixed A_1+A_2 pair of levels. Such A_1+A_2 pairs of levels arise from multiple excitation in the *E* symmetry modes and are subject to *z*–Coriolis interaction governed by a coupling matrix element of the form $Ak\zeta_{\mathrm{eff}}$. In this term, *k* is the signed value for *K* and ζ_{eff} is the Coriolis coupling constant. Due to the high value of the rotational constant *A*, an efficient resonance may possibly occur for one value of *K* only, and this type of interaction may not affect the other subbands. As the energy rises, the vibrational level density increases and these perturbations are expected to become more and more frequent and complex. As demonstrated in the literature, this is indeed the case for the $2\nu_1{}^{12}$ and $3\nu_1{}^{13}$ levels, surrounded by a total density of vibrational states of 66 and 900 states/cm^{-1} respectively. Although it is reasonable to assume that a similar interaction affects the $K=5$ subband of the $3\nu_1+\nu_3+\nu_5$ combination band, it is quite remarkable that only that specific upper level seems to be strongly affected. Indeed, the density of vibrational states in this region is of the order of 10^5states/cm^{-1} (all vibrational symmetries included), and the interaction mechanism just described is expected to have many more opportunities to take place. The peculiarity of this band will be further discussed in Sec. IV.

TABLE V. The spectroscopic parameters of the high-energy component of the $4\nu_1 \leftrightarrow 3\nu_1+\nu_3+\nu_5$ interacting sysem of propyne. Comparison with previous studies and calculated values.

				Calculated values[d]	
Constant (cm^{-1})	Hall[a]	Lin and Reilly[b]	This work[c]	$3\nu_1+\nu_3+\nu_5$	$4\nu_1$
G_ν	12 764.266(5)	12 764.22	12 764.238(1)		
ΔA		-8.52×10^{-4}	$-12.4(1)\times10^{-3}$	-14.2×10^{-3}	0
ΔB	$-4.48(11)\times10^{-3}$	-4.36×10^{-3}	$-4.454(3)\times10^{-3}$	-4.765×10^{-3}	-2.98×10^{-3}
ΔD_J	$-3.78(43)\times10^{-8}$		$-2.48(8)\times10^{-8}$		
ΔD_{JK}			$-2.5(2)\times10^{-6}$		
ΔD_K			fixed to 0		
Lines[c]	93(93)		190(201)		
σ (cm^{-1})			9.0×10^{-3}		

[a]Reference 22. Linear molecule analysis.
[b]Reference 28. Unresolved K structure, ΔA was estimated from the Q branch envelope.
[c]Number of lines used in the fitting procedure with, in parentheses, the total number of lines assigned.
[d]Calculated values of ΔA and ΔB using the experimental values of α^A and α^B given in Table III of Ref 25.
[e]The ground sate rotational constants were constrained to the values (in cm^{-1}) given in Ref. 42: $B_0=0.285\,059\,767$, $A_0=5.308\,304\,457$, $D_J=9.803\,545\,8\times10^{-8}$, $D_{JK}=5.450\,142\,7\times10^{-6}$, and $D_K=0.917\,315\,5\times10^{-4}$.

2. Anharmonic resonance

Table V compares the results of the present rotational analysis for the $3\nu_1+\nu_3+\nu_5$ band with those of the previous literature, which only observed the J-structure.[22,28] The predicted values of ΔA and ΔB calculated from the experimental constants α^A and α^B given in Ref. 25 are also listed in Table V. The value of α_1^A has not been experimentally measured and, as pointed out before, we assumed it to be close to 0 in agreement with force-field calculations.[25] The present values of ΔA and ΔB for the band at 12 764 cm^{-1} are intermediate between those predicted for the unperturbed $4\nu_1$ and $3\nu_1+\nu_3+\nu_5$ levels. They are closer to the values of the $3\nu_1+\nu_3+\nu_5$ state in agreement with the comparison of the observed and predicted energies, thus confirming a moderate mixing of the two interacting levels. The present rotational analysis actually allows the vibrational mixing of the $4\nu_1$ and $3\nu_1+\nu_3+\nu_5$ interacting states to be quantified. The rotational constants of the perturbed combination states are given by

$$A=a^2A_1+b^2A_2, \tag{3}$$

$$B=a^2B_1+b^2B_2, \tag{4}$$

where A_1 and B_1, and A_2 and B_2 are the calculated rotational constants of the unperturbed $3\nu_1+\nu_3+\nu_5$ and $4\nu_1$ states, respectively, and where a and b are the coefficients of the eigenstates in the unperturbed state basis function, such that

$$\varphi_+=a\varphi_1+b\varphi_2, \tag{5}$$

$$\varphi_-=b\varphi_1-a\varphi_2, \tag{6}$$

with $a^2+b^2=1$ and with φ_+ and φ_- related to the eigenstates at higher $(+)$ and lower $(-)$ energy.

Using the predicted values of ΔA and ΔB for the $4\nu_1$ and $3\nu_1+\nu_3+\nu_5$ unperturbed levels, and the presently determined values of ΔA and ΔB for the levels at 12764 cm^{-1} (see Table V), we obtain $a^2=0.87$ and 0.74 by applying Eqs. (3) and (4), respectively. This agreement is reasonable and supports the selected zeroth-order vibrational assignments.

Following the same approach as developed in Ref. 24, the mixing coefficients can also be evaluated by considering the relative intensity of the two bands ($I_{\rm rel}$), provided that the combination band is a fully dark absorption band in a zeroth-order picture: $I_{\rm rel}=b^2/a^2$. As ICLAS does not allow broad absorption features such as the envelope of the band at 12 712 cm^{-1} to be measured, we used an estimation of $I_{\rm rel}=3$ given by Crofton *et al.*[24] from their low-resolution optoacoustic spectrum. The value of a^2 deduced from these intensity considerations is 0.75, in good agreement with the values mentioned above, determined from the rotational constants. The average values of a^2 and b^2 are thus 0.79 and 0.21, respectively.

From the wave numbers of the observed combination ($E_+=12\,764.24\,cm^{-1}$) and overtone ($E_-=12\,712\,cm^{-1}$) levels, it is possible (see Refs. 24 or 30) to calculate the anharmonic interaction matrix element (W_{12}), and the related unperturbed energies E_1^0 ($3\nu_1+\nu_3+\nu_5$) and E_2^0 ($4\nu_1$). The results are $|W_{12}|=21.28\ cm^{-1}$, $E_1^0=12\,753.3\ cm^{-1}$, and $E_2^0=12\,723\ cm^{-1}$. The latter energy is 12 cm^{-1} lower than that extrapolated from the Birge–Sponer plot for the $4\nu_1$ pure stretching level. This deviation is comparable to that observed for the $5\nu_1$ ($-11.0\ cm^{-1}$) and $7\nu_1$ (26.4 cm^{-1}) levels, and may result from extra anharmonic interactions. A more systematic investigation of the whole vibrational energy pattern in propyne, as, e.g., performed in acetylene[8,30] and attempted in ethylene,[49] could bring information relevant to this problem.

The anharmonic resonance coupling between $4\nu_1$ and $3\nu_1+\nu_3+\nu_5$ most likely arises from a third-order potential term of the form $K_{1,35}q_1q_3q_5$, where q_1, q_3 and q_5 are the dimensionless normal coordinates. The corresponding coupling matrix element is

$$\langle \nu_1,\nu_3=0,\nu_5=0|K_{1,35}q_1q_3q_5|(\nu_1-1),\nu_3=1,\nu_5=1\rangle = K_{1,35}\sqrt{\nu_1/8}. \tag{7}$$

Using the value of the coupling matrix element just determined, $|W_{12}|=21.28\,\mathrm{cm}^{-1}$, one can calculate $|K_{1,35}|=30.1\,\mathrm{cm}^{-1}$.

This resonance is expected to systematically induce an intensity transfer from each $n\nu_1$ bright overtone band to the corresponding $(n-1)\nu_1+\nu_3+\nu_5$ combination band, which may become observable on the spectrum. In a first approximation, the $(n-1)\nu_1+\nu_3+\nu_5$ band centers can be predicted using a Dunham expansion

$$G_v=\tilde{\nu}_1(\nu_1-1)+x_{11}(\nu_1-1)^2+\tilde{\nu}_3+\tilde{\nu}_5+x_{35}+(\nu_1-1)(x_{13}+x_{15}), \tag{8}$$

with (in cm^{-1}) $\tilde{\nu}_1=3384.924$ and $x_{11}=-50.289$, determined above, and, from the literature, $\tilde{\nu}_3=2137.87$[45] and $\tilde{\nu}_5=930.28$.[46] To our knowledge, the values of the cross anharmonicities, x_{35} and $(x_{13}+x_{15})$, have not been experimentally determined. Rather than using the recent *ab initio*[50] predicted energies of the $\nu_1+\nu_3$, $\nu_1+\nu_3$, and $\nu_3+\nu_5$, band centers, to calculate x_{13} ($-7.9\ \mathrm{cm}^{-1}$), x_{15} ($0.6\ \mathrm{cm}^{-1}$), and x_{35} ($-1.7\ \mathrm{cm}^{-1}$), we estimated $(x_{13}+x_{15})=-5.67\,\mathrm{cm}^{-1}$ from the unperturbed energy of the $3\nu_1+\nu_3+\nu_5$, and neglected x_{35}. The predicted energies unequivocally point out two weak bands in the spectrum, which were assigned to $\nu_1+\nu_3+\nu_5$ (see the FT spectrum displayed in Fig. 1), and to $2\nu_1+\nu_3+\nu_5$ (see Fig. 3). After several preliminary trial step-by-step calculations, we proceeded to a global fitting using the energy of the $(n-1)\nu_1+\nu_3+\nu_5$ $(n=2-4)$ and $n\nu_1$ $(n=1-3,6)$ sequences of observed levels. The constants $\tilde{\nu}_1$, x_{11}, and $(x_{13}+x_{15})$ were determined while, considering the very limited data set, a number of other constants was constrained: x_{35} to 0, $\tilde{\nu}_3$ and $\tilde{\nu}_5$ to their literature value given above, and $K_{1,35}$ to the value firmly established from the analysis of the $4\nu_1\leftrightarrow 3\nu_1+\nu_3+\nu_5$ dyad ($30.1\ \mathrm{cm}^{-1}$). We obtained (in cm^{-1}) $\tilde{\nu}_1=3383.04$, $x_{11}=-49.90$, and $(x_{13}+x_{15})=-6.43$, in good agreement with the estimations just discussed. The energy levels calculated with these parameters are given in Table III. A rms value of $2.2\ \mathrm{cm}^{-1}$ is achieved on the seven band origins considered, with the maximum deviation ($4.4\ \mathrm{cm}^{-1}$) obtained for $\nu_1+\nu_3+\nu_5$. This kind of agreement probably reflects the crudeness of some approximations, and, possibly, the occurrence of other anharmonic interactions, which we have neglected.

The energy values given in Table III show that, in the sequence of the $n\nu_1$ and $(n-1)\nu_1+\nu_3+\nu_5$ dyads, the minimum energy separation takes place at $n=4$, leading to a maximum intensity transfer in agreement with the observations. The interacting levels within the other pairs are at least $67\ \mathrm{cm}^{-1}$ apart and the coupling then induces a much weaker intensity borrowing and energy shift. In the case of such a weak coupling between nonresonant interacting states, and assuming a strict bright and dark zeroth-order character; the relative intensity of the combination band can be approximated by the square of the ratio of the coupling matrix element by the observed energy separation. This matrix element can be calculated by inserting in Eq. (7) the value of $K_{1,35}$ determined from the $n=4$ dyad. This procedure leads to an intensity, relative to the bright band, of 5.8% for the $2\nu_1+\nu_3+\nu_5$ band and 0.8% for $\nu_1+\nu_3+\nu_5$. These values are in good agreement with the observations, from Figs. 1 and 3, and support the present model and assignments.

E. Hot bands

1. Rotational analysis

The two degenerate bending modes ν_9 ($638.56\ \mathrm{cm}^{-1}$)[47] and ν_{10} ($330.94\ \mathrm{cm}^{-1}$),[48] are responsible for the observation of hot bands. They correspond to the C≡C–H and C–C≡C bends, respectively. At room temperature, the population on the $\nu_{10}=1$ level on one hand and on the $\nu_9=1$ and $\nu_{10}=2$ levels on the other hand, relative to the ground state, is about 40% and 10%. If we denote by s an A_1 nondegenerate vibration mode and by b a bending one (thus $b=9$ or 10), the hot bands are of the type $\nu_s+\nu_b^{\pm 1}-\nu_b^{\pm 1}$. Such bands correspond to so-called biparallel transitions (named BIPARA bands in Ref. 51) and follow $\Delta l=\Delta K=0$ and $\Delta J=0,\pm 1$ selection rules. They are formed by two subbands, one with $l'=l''=1$ with a higher statistical weight for values of $K=1,4,7,...$, and the other with $l'=l''=-1$ with a higher statistical weight for values of $K=2,5,8,...$ The K-dependent part of the transition wave number is governed by the term (see, for instance, Ref. 52)

$$(\Delta A-\Delta B)K^2-2\Delta(A\zeta)Kl_b. \tag{9}$$

In the case of the $3\nu_1+\nu_3+\nu_5+\nu_{10}-\nu_{10}$ hot band, the profile of the J-clumps is observed to consist of a resolved doublet with the strongest component presenting an unresolved shoulder on the blue side. This fine structure is similar in the P and R branches and mostly J-independent. It is clearly observed in the R branch, in Fig. 9, for those lines around $12\,765\ \mathrm{cm}^{-1}$. Our attempts to reproduce this fine structure with realistic values of ΔA, ΔB, and $\Delta(A\xi)$ were unsuccessful, probably indicating significant perturbations. We fitted independently the main and secondary series of peaks in each J-clump, using Eq. (2). The resulting rovibrational parameters $\tilde{\nu}_0$, B' and D_J' are given in Table II. The value of ΔB obtained for the two series of peaks is very close, while the origin of the series is separated by $0.15\ \mathrm{cm}^{-1}$. It seems reasonable to suggest that the $K=0$ transition contributes to the strongest series of peaks, while the other series involves higher K-values. Another, however less probable, interpretation could be the occurrence of an extra anharmonic interaction with a near-resonant state with close value of the B rotational constant.

Two additional hot bands, $3\nu_1+\nu_9-\nu_9$ and $3\nu_1+\nu_{10}-\nu_{10}$, shown in Figs. 3 and 4, were identified and rotationally analyzed. None of them presents a resolved K-structure. The related band origins and B rotational constants are given in Table II. In both cases, the value obtained for ΔB satisfactorily compares with the ΔB value of the cold band.

Finally, we must underline that in the region of the $3\nu_1$ band and to a lesser extent in that of the $3\nu_1+\nu_3+\nu_5$ one, there are several series of regularly spaced lines which could not be assigned. They may arise from perturbation of the K-structure of the main bands or from other hot bands such as $\nu_s+2\nu_{10}-2\nu_{10}$.

TABLE VI. Observed energy shift of hot bands in propyne arising from $\nu_9=1-2$ and $\nu_{10}=1-3$ levels (in (cm^{-1}).

	Cold band center	$\nu_9=1$	$\nu_9=2$	$\nu_{10}=1$	$\nu_{10}=2$	$\nu_{10}=3$
ν_1	3335.07[a]	−21.64[b]		−1.69[c]	−3.4[d]	−5.3[d]
$2\nu_1$	6568.17[e]	−40.79[b]	−81.26[f]	−3.55[b]	−7.07[g]	−10.0[g]
$3\nu_1$	9702.43[h]	−60.36[h]		−5.49[i]	−11.05[j]	
$4\nu_1$	12 711.95[h]	−75[k]				
$3\nu_1+\nu_3+\nu_5$	12 764.24[h]			−9.12[h]		

[a]Reference 25.
[b]Reference 53.
[c]Reference 54.
[d]Reference 55.
[e]Reference 12.
[f]*Q* branch maximum absorption observed in the FT spectrum (Fig. 1).
[g]Reference 56. Note that the values of the band centers given in this reference are systematically redshifted by 0.7 cm^{-1}, however, not affecting the energy shifts.
[h]This work.
[i]Value obtained in this work in perfect agreement with the value given in Ref. 40.
[j]This work. *Q* branch maximum absorption estimated from Fig. 3, confirming the measurement reported as ''doubtful'' in Ref. 40.
[k]Reference 24.

2. Vibrational analysis

In Table VI, we have collected the redshift of the origins of the hot bands relative to the ν_1 and $2\nu_1$ cold bands given in the literature, together with our results for the $3\nu_1$ and $3\nu_1+\nu_3+\nu_5$ manifolds. In Fig. 11, the magnitude of this shift is plotted versus the product $\nu_1\nu_{10}$ for the hot bands arising from $\nu_{10}=1$, 2, and 3. This redshift corresponds to the contribution of the $x_{1,10}\nu_1\nu_{10}$ term. A linear fit of these data leads to determine $x_{1,10}=-1.7975(75)$ cm^{-1} with only one hot band shift excluded from the fit. The magnitude of the cross anharmonicity $x_{1,9}$ was consistently averaged from the $n\nu_1+\nu_9-\nu_9$ band origins ($n=1-3$) to $-20.3(3)$ cm^{-1}. It is thus one order of magnitude larger than $x_{1,10}$.

Using the constants just determined, we could reliably assign to $2\nu_1+2\nu_9-2\nu_9$ a weak *Q* branch which is observed in the FT spectrum (Fig. 1), 81.26 cm^{-1} redshifted from the $2\nu_1$ cold band. We could similarly assign to $4\nu_1+\nu_9-\nu_9$ the weak band reported by Crofton *et al.*[24] at 12 638.0 cm^{-1}. This assignment agrees with the experimental observations from these authors, who reported an important reduction of the band intensity at low temperature. The difference of about 6 cm^{-1} between the predicted (80.2 cm^{-1}) and observed (75 cm^{-1}) redshifts probably results from the partial mixing of the $4\nu_1+\nu_9$ and $3\nu_1+\nu_3+\nu_5+\nu_9$ states through the 1/35 anharmonic interaction mechanism analyzed above.

We can finally analyze the redshift (-9.12 cm^{-1}) of the $3\nu_1+\nu_3+\nu_5+\nu_{10}-\nu_{10}$ hot band at 12 755.13 cm^{-1}. If we neglect the vibrational mixing of the $3\nu_1+\nu_3+\nu_5+\nu_{10}$ and $4\nu_1+\nu_{10}$ levels, this shift then arises from the contribution of the term $3x_{1,10}+x_{3,10}+x_{5,10}$. From the value of $x_{1,10}$ (-1.80 cm^{-1}) determined just above and of $x_{5,10}$ ($+2.38$ cm^{-1}),[57] we obtain $x_{3,10}=-6.09$ cm^{-1}. A more rigorous treatment consisting of considering the 1/35 anharmonic coupling between $3\nu_1+\nu_3+\nu_5+\nu_{10}$ and $4\nu_1+\nu_{10}$ leads to -6.56 cm^{-1}. Both values are in good agreement with an estimation of -7.2 cm^{-1} deduced from the redshift of the $\nu_3+\nu_{10}-\nu_{10}$ band reported in Ref. 58.

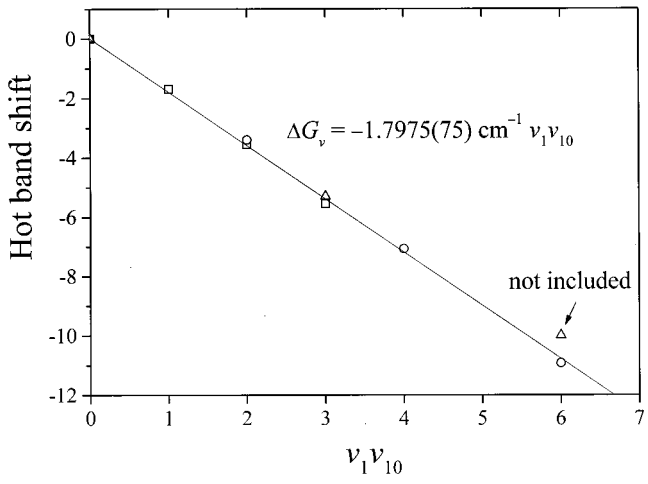

FIG. 11. Plot of the redshift (ΔG_v, in cm^{-1}) of hot bands in propyne arising from the lower states with $\nu_{10}=1$ (square), $\nu_{10}=2$ (circle), and $\nu_{10}=3$ (up triangle). The corresponding values are given in Table VI.

IV. INTRAMOLECULAR VIBRATIONAL REDISTRIBUTION

A. Vibrational homogeneous line broadening of the $6\nu_1$ band

In order to set a reference for the discussion of the linewidths, an iodine line recorded in the same energy region and under similar experimental conditions as the spectrum of propyne is presented in Fig. 12. This reference profile thus provides an upper limit for the instrumental linewidth, which is about 0.04 cm^{-1}. A portion of the *R* branch corresponding to the low *J*-values of the $6\nu_1$ band is also detailed in Fig. 12. This plot clearly evidences that the linewidth of the $R(J)$ clumps is much larger than the instrumental contribution. This broadening could be attributed to the unresolved *K*-fine structure, which gives each *J*-clump a typical linewidth of the order of $(\Delta A-\Delta B)\,J^2$. However, it is critical to notice

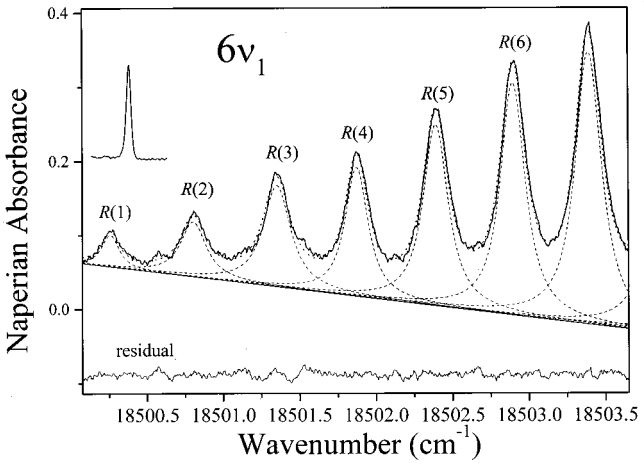

FIG. 12. Fit of the absorbance in base e (αl) of the R branch of the $6\nu_1$ overtone transition of propyne by a sum of lines, each with a Voigt profile. The ICLAS spectrum was recorded at a pressure of 92 hPa with an equivalent absorption pathlength of 15 km. The Voigt profile results from the convolution of the apparatus function and Doppler broadened line profiles with a Lorentzian profile due to IVR. The baseline was adjusted by the fit together with the center, area, and linewidth of each Lorentzian profile. The calculated profile of each $R(J)$ line is plotted with a dashed line and the sum of these line profiles (dotted line) appears to be nearly superimposed with the experimental spectrum. The residual of the fit is given in the lower part of the plot. An upper limit of the width of the spectrograph apparatus function is provided by an absorption line of iodine recorded in the same energy region and presented in the upper left part of the figure.

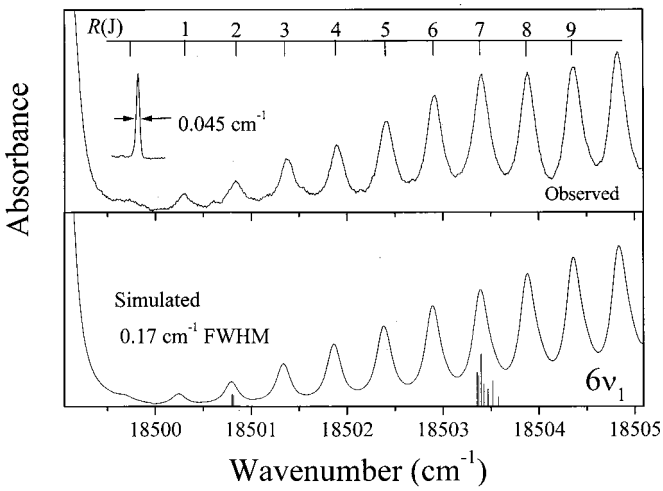

FIG. 13. Comparison of the observed and simulated spectrum for the $R(J)$ lines with wave numbers just above the Q branch, in the $6\nu_1$ overtone transition of propyne. The simulated spectrum was obtained from the rovibrational constant ΔB determined in this work and assuming $\Delta A=0$ (see the text) and by affecting a constant width (FWHM 0.17 cm^{-1}) to the Lorentzian profile of each line. The calculated K-structure is detailed for $R(2)$ and $R(7)$. Note the $R(0)$ line just distinguishable on the wing of the Q branch. An upper limit of the width of the spectrograph apparatus function is provided by an absorption line of iodine recorded in the same energy region and presented in the upper left part of the figure.

that the $R(0)-R(4)$ lines, for which the latter contribution at most similar to the instrumental one, also show an anomalous broadening. This broadening could also be attributed to pressure effects. We have varied the pressure up to 100 Torr and checked that the pressure effect does not significantly contribute to the present case. Therefore, in the absence of extra causes of broadening, one would expect the lines to follow a Gaussian Doppler profile (0.036 cm^{-1} FWHM at room temperature), convoluted with the apparatus function. The resulting total FWHM is predicted to be 0.056 cm^{-1}. This value is at least a factor of 3 lower than observed. We interpret this experimental observation as due to a line fractioning leading to an homogeneous line broadening resulting from IVR from the rotational states in $6\nu_1$ towards the bath of rovibrational states. Such a phenomenon has been observed in propyne and fully resolved for the $3\nu_1$ band (900 states/cm^{-1}), by infrared double-resonance spectroscopy,[13] and for the $2\nu_1$ band (66 states/cm^{-1}), by sub-Doppler infrared laser spectroscopy.[12] The study of the $K=0$ and $0\leqslant J\leqslant 4$ clumps of the $3\nu_1$ level has showed that about 50% of the symmetry-allowed background states were coupled with the $3\nu_1$ state. In the energy region of the $6\nu_1$ state, the total density of vibrational state is much higher, of the order of $10^6/cm^{-1}$. Statistical IVR from the acetylenic CH stretching level energy to a high fraction of the isoenergetic states is therefore expected to take place. As a consequence, there is little hope to individually resolve the fine structure resulting from the statistical fractioning, even at sub-Doppler resolution.

We have recently analyzed the overtone spectrum of the 4_1 band of CHF_3 recorded at room temperature, which exhibits a resolved and unperturbed J-rotational structure affected by homogeneous line broadening due to IVR.[59] The same procedure was followed in the analysis described hereafter. We fitted a number of line profiles in $6\nu_1$ by a sum of independent Lorentzian contributions convoluted with the Doppler profile and the apparatus function. The center position, width, and area of each Lorentzian profile, as well as the baseline, not available experimentally in ICLAS, were adjusted in the fitting procedure. We assumed the baseline to be linear. Figure 12 illustrates the result of this process for the $R(1)$ to $R(7)$ lines. The residuals of the fit are also detailed in Fig. 12. It appears that the profiles of the J-clumps are fully symmetric and well described by a Lorentzian function. This result is confirmed for higher J-values, including $P(J)$ lines not obscured by the Q branch degraded to the red. An interesting feature is that, in the limit of experimental uncertainty, the Lorentzian linewidths are almost J-independent with an average value of 0.17 cm^{-1}. For comparison, we have simulated the $6\nu_1$ spectrum using the term formula given in Eq. (1) and the rotational constants A' and B' previously discussed, also including the line profiles just discussed. The agreement, illustrated in Fig. 13, is excellent. Even the very weak $R(0)$ line superimposed on the high-energy wing of the Q branch is satisfactorily reproduced.

As a summary, the main features revealed by the detailed study of the $6\nu_1$ band are: (i) the observation of a resolved J-fine structure, (ii) the absence of perturbation in this structure, (iii) the existence of an homogeneous line broadening effect, and (iv) the universal role of a phenomenological Lorentzian line profile with 0.17 cm^{-1} FWHM to quantatively account for IVR.

B. IVR mechanism

The famous model of Bixon and Jortner[60] makes the connection between the concepts of line energy fractioning and decay rates. This model also states that a Lorentzian line profile is expected when the bath of rovibrational states strongly interacts with the zeroth-order bright state, and therefore significantly contributes to the composition of the eigenstate involved in the excitation process. The corresponding linewidth is then given by the Fermi golden rule

$$\Gamma = 2\pi \langle V^2 \rangle \rho, \tag{10}$$

where $\langle V^2 \rangle$ is the mean value of the square of the coupling and ρ is the density of states interacting with the bright state. The density of states in propyne, calculated including the full set of diagonal anharmonicities compiled in Ref. 61, is $10^6/\mathrm{cm}^{-1}$ at the energy of $6\nu_1$ ($18\,500\ \mathrm{cm}^{-1}$). This density is based on a total count, thus including the A_1, A_2, and E symmetry states, in the proportion 1:1:2.

The independence of the measured linewidth with the J-rotational quantum number, which we highlighted in the previous section, is a signature of the anharmonic nature of the coupling of the $\nu_1=6$ state with the bath states. Any Coriolis-type interaction would indeed have proven to depend on the rotational quantum numbers J and K. The eigenstate-resolved spectroscopy of the $3\nu_1$ band shows a dramatic increase of the line fractioning with J.[13] However, in the same investigation, Gambogi *et al.* also show that, for a given value of K, the decay rate which measures the total width of the J clumps is largely independent of J. These authors interpreted this feature as resulting from two combined and opposite effects: the increase of the density of lines with $(2J'+1)$ and a decrease of the averaging coupling matrix element as $1/(2J'+1)$. The latter effect was considered in detail for the $K=0$ states and attributed to the decrease of the $K=0$ character of the bath states because of their strong mixing with states with higher K-values, by xy Coriolis or centrifugal couplings. However, the important increase of the decay rate measured between $K=0$ and $K=1$ states was thought to result from the existence of a so-called doorway state which is coupled to the bath states by z-axis Coriolis interaction or tuned closer to resonance at $K=1$ than at $K=0$. In the present case, we do not have any evidence of a strong K-dependence of the coupling strength with the bath. It appears that, limiting our discussion to the $\nu_1=6$ state, a direct anharmonic coupling of the $6\nu_1$ state with a significant fraction of the near resonant A_1 states of the bath is consistent with the observed line profile. In the case of the $3\nu_1$ level, approximately 50% of the background states with the adequate symmetry, (A_1), were coupled with the bright state.[13] In the region of the $\nu_1=6$ state, the density of A_1 states in the range is $1/6\ 10^6/\mathrm{cm}^{-1}$. If we assume the full density of A_1 dark states to be coupled with the $6\nu_1$ bright state, using the Fermi golden rule [Eq. (11)] and the universal homogeneous linewidth extracted from the study of the line profiles, we can calculate the root mean square interaction matrix element to be $\sqrt{\langle V^2 \rangle} = 4.0 \times 10^{-4}\ \mathrm{cm}^{-1}$ for $K=0$, compared to $8 \times 10^{-3}\ \mathrm{cm}^{-1}$ for $K=0$ in the $3\nu_1$ level.[13]

C. The doorway states

The structure of the acetylenic CH overtone bands presents dramatic changes from one band to another. Indeed, the rotational structure is resolvable for the first $n\nu_1$ overtone transitions $(n=1-3)$, partly lost for $n=4$, absent for $n=5$, homogeneously broadened at $6\nu_1$, and again resolved at $7\nu_1$.[22] This situation is thus fully independent of the vibrational state density, which is uniformly increasing with the energy. It rather suggests a mode-specific coupling mechanism with the bath of vibrational states. A strong hierarchy seems to hold in the strength of the couplings, indicating that the dynamics of high vibrational overtone levels is controlled by an extremely sparse set of doorway states. This statement is supported by a more detailed examination of two different sets of results.

The $4\nu_1$ manifold, in the first place, is particularly interesting. Two bands are observed, as we have previously discussed. The higher-energy component mostly corresponds to the $3\nu_1+\nu_3+\nu_5$ level, moderately mixed ($a^2=0.79$) with the $4\nu_1$ state. It presents a rather unperturbed fine structure with no significant homogeneous line broadening. The other component, of dominant $4\nu_1$ character, exhibits, on the contrary, broadened and only partly resolved lines, superimposed to a strong unresolved broadband absorption (see Fig. 8). A simulation similar to the one detailed for the $6\nu_1$ band presented above indicates that a homogeneous line broadening of at least $1\ \mathrm{cm}^{-1}$ FWHM is required to wash out the J-rotational structure as observed in the spectrum of Fig. 8. This observation is dramatically different from the situation in the nearby combination state $(3\nu_1+\nu_3+\nu_5)$ and contradicts the standard rule that a combination state is more subject to couplings than a pure overtone state. One might indeed expect more possibilities of coupling for the combination level than for the CH stretch and a partial transfer, only, of these couplings to the overtone level through anharmonic mixing of the two zero-order states. The experimental results show that the situation is exactly opposite. This unusual phenomenon was first evidenced in the low overtone region of propyne[26,27] where the pure acetylenic stretching states are more subject to IVR than the nearly isoenergetic combination states. A similar observation has recently been reported by Boyarkin *et al.* in methanol,[21] involving anharmonically coupled OH stretch overtones and combination states including the CH stretchings. These authors attribute the dramatic difference of the fragmentation they observe in the two bands to the nonuniform distribution of the background states which are possibly coupled to the two eigenstates by low-order anharmonic terms. The couplings would thus differently affect each of the two eigenstates in a dyad. In the present case, however, the density of vibrational states of adequate symmetry is one order of magnitude higher than in methanol ($1130/\mathrm{cm}^{-1}$ instead of $122/\mathrm{cm}^{-1}$). In consequence, the distribution of the background states ought to present a more statistical and thus uniform character with fewer gaps and fewer regions with clumps. Another mechanism therefore probably holds for propyne, which we thus suggest to be highly mode specific.

Second, it is interesting to consider the hot bands. The $3\nu_1+\nu_3+\nu_5+\nu_{10}-\nu_{10}$ hot band shows no evidence of ho-

mogeneous broadening, within the present instrumental resolution. On the other hand, we are unable to resolve any fine structure in the $4\nu_1+\nu_{10}-\nu_{10}$ and $5\nu_1+\nu_{10}-\nu_{10}$ hot bands which are expected to be superimposed on the envelope of the broad $4\nu_1$ and $5\nu_1$ bands, respectively. The characteristics of the hot bands thus closely follow those of the corresponding cold bands, $3\nu_1+\nu_3+\nu_5$, $4\nu_1$ and $5\nu_1$. There is no reason to believe that accidental resonance or detuning with the possible doorway states observed for the upper levels of the cold band should be preserved for the upper levels of the hot bands which have an energy increase of about 331 cm^{-1}. Indeed, due to the contribution of the cross anharmonicity term $x_{s,10},\nu_s\nu_{10}$ to the energy, the *resonant* vibrational environment in the vicinity of the upper level of the hot bands may be quite different from that of the upper level of the cold band. That clearly indicates that IVR involves *off-resonance* vibrational coupling between the pure overtone level and the doorway state. This specific mechanism is thus simply transferred to the related pair of states containing an additional quantum of excitation in the ν_{10} mode, this mode behaving as a ''spectator.'' These observations fully agree with the conclusions derived by Markus *et al.* from their quantum calculations.[11]

In the $n=4$ dyad, the strong difference in the fractioning of the wave functions φ_+ and φ_- defined in Eqs. (5) and (6) may be due to a more efficiently tuned resonance of this specific doorway state with φ_- than with φ_+. It could also be attributed to an important difference in the coupling matrix elements induced by the difference either in the amplitude or the sign in the eigenvector expression. The high peculiarity of the $3\nu_1+\nu_3+\nu_5$ band (φ_+) could result in an accidental cancellation of the interaction matrix element between the doorway state and the state φ_+ (and not φ_-) by virtue of the relative signs of *a* and *b* in Eqs. (5) and (6). This situation is, however, highly unlikely.

These various features strongly suggest that a low-order interaction with a very specific sequence of off-resonant doorway states is appropriate for describing the observations in propyne. This interaction mechanism presents a maximum coupling strength occurring for $\nu_1=4$ and 5, probably resulting from an optimum tuning of the resonance. The identification of these doorway states remains an open question.

V. CONCLUSION

The present high-resolution exploration of the acetylenic CH stretch $n\nu_1$ overtone bands from $n=2$ up to $n=6$ has allowed us to improve the spectroscopy of the corresponding upper levels, to evidence a systematic 1/35 anharmonic interaction and to give more insight to the hierarchy of couplings connecting the acetylenic CH stretch to the dense vibrational background. The assignment of the dyad near 12 750 cm^{-1} to $4\nu_1$ and $3\nu_1+\nu_3+\nu_5$ previously proposed by Crofton *et al.*[24] has been fully confirmed from (i) the rotational analysis, (ii) the observation of two (weaker) similar combination bands borrowing their intensity from the $2\nu_1$ and $3\nu_1$ bands through the same 1/35 interaction mechanism, and (iii) the analysis of the redshift of the $3\nu_1+\nu_3+\nu_5+\nu_{10}-\nu_{10}$ hot band.

The $n=4$ dyad shows a very peculiar situation with a mostly unperturbed combination level in anharmonic interaction with a CH stretch level much less isolated from the vibrational bath. The two interacting levels are separated by about 15 cm^{-1}, while the homogeneous line broadening is estimated to be at least of the order of 1 cm^{-1} for the (mixed) $4\nu_1$ eigenstate and is not evidenced for the (mixed) $3\nu_1+\nu_3+\nu_5$ eigenstate. Translated into the time domain, it implies a clear separation of time scales of at least 1 or 2 orders of magnitude between the first and second steps of IVR from the $4\nu_1$ level. Although limited to this particular dyad, the situation is very similar to the one encountered in CHF_3 where a Fermi resonance stretch–bend polyad system shows some specific and limited homogeneous broadening for each level of the polyad leading to a separation of time scales of as much as 3 orders of magnitude.[9,19] In the case of the $6\nu_1$ stretching level, the energy decay, $\tau=(2\pi c\Gamma)^{-1}$, deduced from the 0.17 cm^{-1} linewidth is not faster than 10 ps as a consequence of the very weak average coupling with the dense vibrational background.

The present study over a broad energy region was performed by using a wide variety of absorption techniques. Among these, we have presented the first spectroscopic application of two newly developed ICLAS systems. One is using multiple quantum wells structure in VECSEL configuration.[32] This is a very promising development which can extend ICLAS in the near- and mid-infrared range with a broad and easy wavelength tunability and possible application for trace detection. The second is a Ti: Sapphire laser in a new ring configuration providing higher sensitivity in the entire tuning range of this crystal.[31]

ACKNOWLEDGMENTS

T. Rizzo (EPFL, Lausanne) is thanked for communicating a preprint of Ref. 21 prior to publication. J.-P. Booth (LSP, Grenoble) is acknowledged for the loan of the excimer laser used for the CRDS experiment, as is R. Planel (CNET, Bagneux) for providing us the multiple quantum wells structure. N. Ignascio (Grenoble) is acknowledged for a preliminary calibration and analysis of the $6\nu_1$ band. M.H. acknowledges financial support from the Fonds National de la Recherche Scientifique (FNRS-Belgium) and the ULB. A.C. and M.H. are indebted to the CNRS and FNRS/CGRI for a collaborative research grant.

[1] K. K. Lehmann, B. H. Pate, and G. Scoles, Annu. Rev. Phys. Chem. **45**, 241 (1994).
[2] K. K. Lehmann, M. Herman, and I. M. Mills, guest editors, Overtone Spectrosccopy Dynamics, Chem. Phys, special issue **190**, 157 (1995).
[3] R. W. Field, J. P. O'Brien, M. P. Jacobson, S. A. B. Solina, W. F. Polik, and H. Ishikawa, Adv. Chem. Phys. **101**, 463 (1997).
[4] L. Halonen, Adv. Chem. Phys. **104**, 1 (1999).
[5] M. Quack, Annu. Rev. Phys. Chem. **45**, 241 (1994).
[6] D. J. Nesbitt and R. W. Field, J. Phys. Chem. **100**, 12735 (1996).
[7] F. F. Crim, Annu. Rev. Phys. Chem. **44**, 397 (1993).
[8] M. I. El Idrissi, J. Liévin, A. Campargue, and M. Herman, J. Chem. Phys. **110**, 2074 (1999).
[9] J. Segall, R. N. Zare, H. R. Dübal, M. Lewerenz, and M. Quack, J. Chem. Phys. **86**, 634 (1987).
[10] J. E. Baggott, M. C. Chuang, R. N. Zare, H.-R. Dübal, and M. Quack, J. Chem. Phys. **82**, 1186 (1985); H.-R. Dübal and M. Quack, *ibid.* **81**, 3779 (1984); A. Amrein, H.-R. Dübal, and M. Quack, Mol. Phys. **56**, 727

(1985); J. S. Wong, W. H. Green, Jr., C. Cheng, and C. B. Moore, J. Chem. Phys. **86**, 5994 (1987); M. Hippler and M. Quack, Ber. Bunsenges. Phys. Chem. **99**, 417 (1995).
[11] A. A. Stuchebrukhov and R. A. Marcus, J. Chem. Phys. **98**, 6044 (1993); A. A. Stuchebrukhov, A. Mehta, and R. A. Marcus, J. Phys. Chem. **97**, 12491 (1993); A. Mehta, A. A. Stuchebrukhov, and R. A. Marcus, *ibid.* **99**, 2677 (1995).
[12] A. Mcllroy, D. J. Nesbitt, E. R. Th. Kerstel, B. H. Pate, K. K. Lehmann, and G. Scoles, J. Chem. Phys. **100**, 2596 (1994); A. Mcllroy and D. J. Nesbitt, *ibid.* **92**, 2229 (1990); M. Chevalier and A. De Martino, *ibid.* **90**, 2077 (1989); A. de Martino, R. Frey, and F. Pradère, Mol. Phys. **55**, 731 (1985).
[13] J. E. Gambogi, E. R. Kerstel, K. K. Lehmann, and G. Scoles, J. Chem. Phys. **100**, 2612 (1994).
[14] R. H. Page, Y. R. Shen, and Y. T. Lee, J. Chem. Phys. **88**, 5362 (1988), *ibid.* **88**, 4621 (1988).
[15] S. L. Coy and K. K. Lehmann, J. Chem. Phys. **84**, 5239 (1986).
[16] T. R. Rizzo, C. C. Hayden, F. F. Crim, and X. Luo, J. Chem. Phys. **81**, 4501 (1984); L. J. Butler, T. M. Ticich, M. D. Likar, and F. F. Crim, *ibid.* **81**, 4501 (1984); X. Luo, P. R. Fleming, T. A. Seckel and T. R. Rizzo, *ibid.* **93**, 9194 (1990), and references cited therein; X. Luo and T. R. Rizzo, *ibid.* **94**, 889 (1991).
[17] M. Hippler and M. Quack, Chem. Phys. Lett. **231**, 65 (1994); J. Chem. Phys. **104**, 7426 (1996).
[18] T. Arusi-Parpar, R. P. Schmid, Y. Ganot, I. Bar, and S. Rosenwaks, Chem. Phys. Lett. **287**, 347 (1998), and references therein; R. P. Schmid, T. Arusi-Parpar, R.-J. Li, I. Bar, and S. Rosenwaks, J. Chem. Phys. **107**, 385 (1997).
[19] O. Boyarkin, R. D. F. Settle, and T. R. Rizzo, Ber. Bunsenges. Phys. Chem. **99**, 504 (1995).
[20] R. D. F. Settle and T. R. Rizzo, J. Chem. Phys. **97**, 2823 (1992); O. V. Boyarkin and T. R. Rizzo, *ibid.* **105**, 6285 (1996).
[21] O. Boyarkin, T. R. Rizzo, and D. Perry, J. Chem. Phys. **110**, 11359 (1999).
[22] R. R. Hall, Ph.D. thesis, Rice University, Texas (1984).
[23] L. Baylor, E. Weitz, and P. Hofman, J. Chem. Phys. **88**, 7434 (1988).
[24] M. W. Crofton, C. G. Stevens, D. Klenerman, J. H. Gutow, and R. N. Zare, J. Chem. Phys. **89**, 7100 (1988).
[25] E. R. Kerstel, K. K. Lehmann, B. H. Pate, and G. Scoles, J. Chem. Phys. **100**, 2588 (1994).
[26] J. E. Gambogi, J. H. Timmermans, K. K. Lehmann, and G. Scoles, J. Chem. Phys. **99**, 9314 (1993).
[27] J. Go and D. S. Perry, J. Chem. Phys. **97**, 6994 (1992); J. Go, T. J. Cronin, and D. S. Perry, Chem. Phys. **175**, 127 (1993).
[28] Z. Lin, K. Boraas and J. P. Reilly, J. Mol. Spectrosc. **156**, 147 (1992).
[29] A. Campargue, M. Chenevier, and F. Stoeckel, Spectrochim. Acta Rev. **13**, 190 (1990).
[30] M. Herman, J. Liévin, J. Vander Auwera, and A. Campargue, Adv. Chem. Phys. **108**, 1 (1999).
[31] A. Kachanov and A. Garnache (unpublished).
[32] A. Garnache, A. A. Kachanov, F. Stoeckel, and R. Planel, Opt. Lett. **24**, 826 (1999); A. Garnache, A. A. Kachanov, F. Stoeckel and R. Houdré (submitted).
[33] L. S. Rothman, C. P. Rinsland, A. Goldman, S. T. Massie, D. P. Edwards, J.-M. Flaud, A. Perrin, C. Camy-Peyret, V. Dana, J. Y. Mandin, J. Schroeder, A. McCann, R. R. Gamache, R. B. Wattson, K. Yoshino, K. V. Chance, K. W. Jucks, L. R. Brown, V. Nemtchinov, and P. Varanasi, J. Quant. Spectrosc. Radiat. Transf. **60**, 665 (1998).
[34] S. Gerstenkorn and P. Luc, ''Atlas du spectre d'absorption de la molécule d'iode,'' Edition du CNRS, Paris, 1978.
[35] A. O'Keefe and D. A. G. Deacon, Rev. Sci. Instrum. **59**, 2544 (1988).
[36] D. Romanini, in *Cavity-Ringdown Spectroscopy—An Ultratrace-Absorption Measurement Technique*, Kenneth W. Busch and Marianna A. Busch, editors (American Chemical Society, Washington, DC, 1998).
[37] D. Romanini, A. A. Kachanov, F. Stoeckel, Chem. Phys. Lett. **270**, 538 (1997).
[38] D. Romanini, A. A. Kachanov, and F. Stoeckel, Chem. Phys. Lett. **270**, 546 (1997).
[39] D. Romanini, L. Biennier, F. Salama, A. A. Kachanov, L. J. Allamandola, and F. Stoeckel, Chem. Phys. Lett. **303**, 165 (1999).
[40] G. Herzberg, F. Patat, and H. Verleger, J. Phys. Chem. **41**, 123 (1937).
[41] R. M. Badger and S. H. Bauer, J. Chem. Phys. **5**, 599 (1937).
[42] A. Lesarri, M. E. Carro, R. M. Villamañan, D. G. Lister, J. C. López, and J. C. Alonso, J. Mol. Spectrosc. **149**, 317 (1991).
[43] N. F. Henfrey and B. A. Thrush, J. Mol. Spectrosc. **113**, 426 (1985).
[44] N. F. Henfrey and B. A. Thrush, J. Mol. Spectrosc. **121**, 139 (1987).
[45] N. F. Henfrey and B. A. Thrush, J. Mol. Spectrosc. **121**, 150 (1987).
[46] P. Pracna, J. Demaison, G. Wlodarzack, A. Lesarri, and G. Graner, J. Mol. Spectrosc. **177**, 124 (1996).
[47] K. Pekkala, G. Graner, G. Wlodarzack, and J. Demaison, J. Mol. Spectrosc. **149**, 214 (1991).
[48] G. Graner and G. Wagner, J. Mol. Spectrosc. **144**, 389 (1990).
[49] R. Georges, M. Bach, and M. Herman, Mol. Phys. **97**, 279 (1999).
[50] B. Schulz and P. Bostchwina, Mol. Phys. **89**, 1553 (1996).
[51] G. Graner and H. Bürger in *Vibration-Rotational Spectroscopy and Molecular Dynamics 3*, edited by D. Papousek (World Scientific, Singapore, 1997).
[52] F. Meguellati, G. Graner, K. Burczyk, and H. Bürger, J. Mol. Spectrosc. **185**, 392 (1997).
[53] R. Anttila, S. Jaakkonen, and T. Sahlström, Spectrochim. Acta A **28A**, 1615 (1972).
[54] J. W. Russell, M. Murphy, T. R. Faulkner, and S. Sugai, Spectrochim. Acta A **27A**, 119 (1971).
[55] R. W. Bayer and W. F. Edgell, J. Chem. Phys. **37**, 2502 (1962).
[56] R. K. Thomas and H. W. Thompson, Spectrochim. Acta A **24A**, 1337 (1968).
[57] T. Al Adlouni and G. Graner, J. Mol. Spectrosc. **127**, 186 (1988).
[58] D. R. Boyd and B. W. Thompson, Trans. Faraday Soc. **48**, 493 (1952).
[59] D. Romanini and A. Campargue, Chem. Phys. Lett. **254**, 52 (1996).
[60] M. Bixon and J. Jortner, J. Chem. Phys. **48**, 715 (1968).
[61] A. Mcllroy and D. J. Nesbitt, J. Chem. Phys. **91**, 104 (1989).